scientific reports

Check for updates

OPEN

Functional discrimination of CSF from Alzheimer's patients in a brain on chip platform

Louise Miny[1,3], Jessica Rontard[1], Ahmad Allouche[4], Nicolas Violle[4], Louise Dubuisson[1], Aurélie Batut[1], Alexandre Ponomarenko[1], Rania Talbi[1], Hélène Gautier[1], Benoît G. C. Maisonneuve[1], Serge Roux[1], Florian Larramendy[1], Thibault Honegger[1]✉ & Isabelle Quadrio[2,3]✉

Neurodegenerative diseases, including Alzheimer's disease (AD), present significant diagnostic challenges due to overlapping symptoms and the invasive, time-consuming, and costly nature of current diagnostic methods. While AD remains the only neurodegenerative disorder for which biomarkers in cerebrospinal fluid (CSF), such as amyloid beta peptide (Aβ), are available for clinical diagnosis, similar tools are lacking for other neurodegenerative conditions. This diagnostic gap hinders timely and accurate differential diagnoses, limiting patient access to appropriate clinical trials and therapeutic interventions. In this study, we developed a compartmentalized microfluidic platform to facilitate differential diagnosis of neurodegenerative diseases by providing an initial screening tool to guide patients toward targeted clinical pathways. Using CSF samples from AD patients with confirmed diagnoses, we showed a proof of concept to distinguish between non neurodegenerative (NN) and Alzheimer's samples. Human glutamatergic neurons derived from induced pluripotent stem cells (iPSCs) were exposed to synthetic Aβ oligomers (AβO) and patient CSF to assess their effects on neuronal network activity. Neuronal responses were recorded via microelectrode array (MEA) before and after treatments, with tetrodotoxin (TTX) serving as a control for validating modulation of the neuronal network. Our findings demonstrated that key electrophysiological metrics extracted from MEA recordings can tend to differentiate AD from non-neurodegenerative CSF samples. This standardized platform not only provides a robust approach for AD biomarker validation but also offers a foundation for broader differential diagnosis of neurodegenerative diseases. By enabling more accurate patient stratification, this tool could have the potential to direct patients toward appropriate clinical trials, enabling the diagnosis of a broader range of neurodegenerative diseases. This approach has the potential to expand the patient population included in research and accelerate the development of new therapeutic strategies.

Neurodegenerative diseases, including Alzheimer's disease (AD), represent a major global health challenge. AD is the leading cause of dementia worldwide and is characterized by the accumulation of aggregated amyloid-beta peptide (Aβ) in neurons, leading to synaptic dysfunction and neuronal death[1–4]. While extensively studied for decades, the diagnosis of AD remains complex and often relies on a combination of clinical examination, neuropsychological testing, and brain imaging. In atypical cases, core biomarkers of AD pathology, such as cerebrospinal fluid (CSF) Aβ levels, can assist in establishing the diagnosis and identifying the etiology[5–7]. However, these diagnostic methods are time-consuming and expensive. Additionally, they often fail to account for differential diagnoses, resulting in delayed or inaccurate conclusions. This diagnostic challenge impacts the timely care of patients and hinders efforts to address the broader spectrum of neurodegenerative diseases[8].

To improve diagnostic capabilities, researchers have sought innovative technologies for detecting disease-specific biomarkers in biological fluids[9–12]. Despite progress, the incomplete understanding of the underlying mechanisms of neurodegenerative diseases and the complexity of CSF composition limit the development of accurate diagnostic tools. Moreover, most neurodegenerative disorders, apart from AD, lack specific biomarkers measurable in biological fluids, further complicating their diagnosis and differentiation.

[1]NETRI, Lyon, France. [2]Biochemistry and Molecular Biology Department, Neurodegenerative Pathologies, LBMMS, 59 Boulevard Pinel, Bron, Hospices Civils de Lyon, 69500 Lyon, France. [3]Lyon Neurosciences Research Center, BIORAN Team, 59 Boulevard Pinel Bron, CNRS UMR 5292, INSERM U1028, 69500 Lyon, France. [4]ETAP-Lab, Vandoeuvre-Lès-Nancy, France. ✉email: thibault.honegger@netri.com; isabelle.quadrio@chu-lyon.fr

Microfluidic technologies have emerged as a powerful tool for studying and detecting biomarkers of neurological diseases using biological fluids[13–15]. For example, Koch et al. (2019) demonstrated the ability to discriminate CSF from healthy patients and those with autoimmune encephalitis (AE) using a microfluidic device coupled with a microelectrode array (MEA)[16–19]. MEA-based electrophysiological recordings are widely employed in in vitro neurological studies to assess the functionality, maturity, and network dynamics of neurons in microfluidic devices. However, most existing studies focus on single-device recordings, limiting their applicability for large-scale differential diagnostic screening[20–24].

In compartmentalized microfluidic devices, neurons could respond to stimuli or biological samples applied to specific compartments. This approach allows precise control of the microenvironment and enables the study of how a stimulus or pathological sample in one compartment affects the activity of interconnected neuronal networks. By monitoring changes in neuronal activity, this system could provide critical insights into the differentiation of neurodegenerative diseases and guide the development of targeted therapies.

In this study, we aimed to demonstrate the potential of a high-throughput (HTS) organ-on-chip platform to discriminate between neurodegenerative diseases. Specifically, we evaluated whether human neurons derived from induced pluripotent stem cells (hiPSCs) could act as biosensors for differential diagnosis. First, glutamatergic and GABAergic neurons were cultured in compartmentalized HTS devices, and their functional activity was characterized using electrophysiological recordings. TTX, a sodium channel inhibitor, and synthetic Aβ oligomers were applied as controls to validate the platform's functionality. Finally, CSF from non-neurodegenerative and AD patients was introduced to human glutamatergic neurons, and key electrophysiological metrics were extracted to distinguish between non neurodegenerative and AD CSF samples. This platform represents a promising tool for improving the differential diagnosis of neurodegenerative diseases, guiding patients toward appropriate clinical trials, and accelerating the development of new therapeutic strategies.

Results

An Organ on chip platform for high-throughput electrophysiological recording of compartmentalized neural networks

To simultaneously record neurons co-cultures, a microfluidic platform composed of 16 microfluidic devices coupled with MEA in a standard high throughput design, named DuaLink MEA, was developed and manufactured (Fig. 1a). Microfluidic devices are made of Polydimethylsiloxane (PDMS) (Fig. 1b). Devices are composed of inlets and outlets, used to seed cells and adding compounds, and three compartments linked with microchannels allowing fluidic isolation. The dimensions of both cell culture channels are 18,800 (Length) ×1000 (Width) ×200 (Height) µm, and microchannels are 125 (Length) ×6 (Width) ×3 (Height) µm (Figure S1)). This architecture allows neurons to be seeded in the cell culture compartment (channel 1) while only neurites can grow throughout microchannels to reach the opposite cell culture (in channel 3) (Fig. 1c). Moreover, microfluidic devices were directly bonded on a MEA sheet developed by Axion Biosystems allowing neurons to be in direct contact with electrodes. (Fig. 1c). All regions of the neuronal network were recorded: 15 electrodes were placed in both channels 1 and 3 (Ch1 and Ch3), 5 electrodes in the inter-microchannels (1µ2 and 2µ3), and 2 electrodes in channel 2 (Ch2) (Fig. 1c). For easier interpretation of the results presented in this paper, the electrodes were color-coded according to their position under the device (each compartment/set of microchannels having its specific color, as depicted in Fig. 1d. Compartmentalization allowed us to investigate functional activity across neurons and neuronal network (Fig. 1d). This specific positioning of electrodes allowed us to record various neuronal components, including neuronal culture in channels as well as their axons and dendrites in microchannels. Microchannels specifically enabled the isolation of axons and neurites and the precise recording of action potential between channels. Thanks to the transparency of the PDMS and the MEA sheet, the neuronal network organization and composition were investigated using immunofluorescence assay.

Neurons hiPSC derived in microfluidic devices are mature and present spontaneous activity

Human glutamatergic and GABAergic neurons derived from iPSCs were seeded in DuaLink MEA's Ch1 and Ch3, respectively. Using adapted provider protocols to ensure full differentiation and maturation prior to

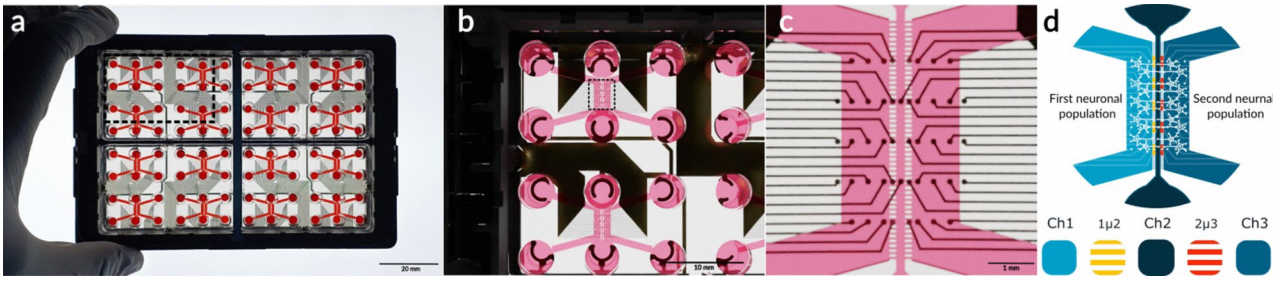

Fig. 1. Microfluidic platform by NETRI with Axion Biosystem's technology. (**a**) Pictures of the NeoBentoPRO composed of four QuarterBento and sixteen microfluidic chips. (**b**) Realistic rendering of zoomed QuarterBento of four DuaLink chip MEA. (**c**) Realistic rendering of a detailed DuaLink chip MEA showing three culture compartments. Black dots represent microelectrodes placed below the chip. (**d**) Schematic representation of DuaLink MEA with compartmentalized neuronal culture with one cell type seeded in Ch1 and the other cell type seeded in Ch3, axonal propagations are respectively in microchannels 1µ2 and 2µ3.

performing subsequent experiments, they were maintained for 21 days and supplemented with fresh media to achieve full maturation between day 19 and day 21. Brightfield pictures were taken to monitor the evolution of neurons and their connection over time (Fig. 2b). Neuronal structure and functional activity were confirmed with immunofluorescence assay at day 21 and electrophysiological recordings of spontaneous activity at days 7, 14, and 21. Moreover, neuronal viability in microfluidic device were evaluated at the end of the culture with Live/dead assays with quantification (Fig. 2a). As expected from the cell providers' protocols, the viability of the glutamatergic and GABAergic neurons at day 21 was 46.7 (± 8.4) % and 49.5 (± 10.2) %, respectively (n = 20) (Fig. 2c). There was no significant difference of the live cells' percentage between glutamatergic and GABAergic neurons (Fig. 2f). To ensure the full differentiation of iPSC in neurons, pluripotency and specific markers were quantified by immunofluorescence at day 21 (n = 10 per markers) (Fig. 2d,e). Pluripotency markers (Sox2 and Nestin) stained respectively 4.7 (± 4.9) % and 1.5 (± 2.4) % of the glutamatergic neurons, and 9.7 (± 12.6) % and 4.2 (± 6.5) % of the GABAergic neurons. They were both inferior to 10%, indicating that cells were differentiated (Fig. 2g). β-III tubulin, a specific neuronal marker, stained 85.2 (± 6.7) % of the glutamatergic population and 78.1 (± 19.3) % of the GABAergic population. For both neuronal types, vGlut1 (glutamatergic specific marker) and GABA (GABAergic specific marker) stained respectively 84.3 (± 18.1) % and 3.8 (± 4.1) % of glutamatergic neurons, and 2.1 (± 2.9) % and 69.4 (± 3.8) % of GABAergic neurons (Fig. 2h). We confirmed that most of the neurons presumed to be glutamatergic are indeed glutamatergic, and those presumed to be GABAergic are indeed GABAergic. Similarly, neurons presumed to be GABAergic were verified by the presence of the GABA marker, confirming their identity as GABAergic neurons. Finally, the neuronal co-culture recorded at day 7, 14 and 21 allows to plot raster graphs showing a global observation of the total recording over time on all electrodes. They showed an increase of detected action potential, represented by compartments color-coded points, over time (Fig. 2i). The recorded activity in the channels over time is represented by mean firing rate (MFR) and weighted mean firing rate (WMFR, i.e. number of spikes per seconds on active electrodes). WMFR showed a tendency to increase between day 7 (n = 56) and day 14 (n = 56). WMFR becomes statistically significant in microchannels between day 14 (n = 56) and day 21 (n = 56) ($p < 0.0001$). At day 21, WMFR was increased in microchannels compared to channels ($p < 0.0001$) (Fig. 2j). Synchrony of both glutamatergic and GABAergic neurons was also measured. A significant rise of synchrony index, generally comprised between 0 and 1, was observed between day 14 and day 21 in microchannels 1µ2 (respectively n = 28 and n = 43) ($p < 0.01$) and in microchannels 2µ3 (respectively n = 29 and n = 42) ($p < 0.0001$) and in the channel 3 (respectively n = 25 and n = 42) ($p < 0.05$) (Fig. 2k).

Chemical inhibitor added in a single compartment has an impact over the electrical activity of the entire network

For all further experiments, we used the DuaLink MEA in which glutamatergic neurons were seeded in both Ch1 and Ch3, while neurites could go through 1µ2 and 2µ3 respectively (Fig. 2b). By using the same neuronal culture in both channels but only adding drug compound in one, we could assess with more accuracy the drug's impact on synaptic connectivity and network activity, isolating the effects on excitatory transmission without the influence of inhibitory signalling from GABAergic neurons. This approach allowed us to gain clearer insights into the drug's mechanism of action within a controlled excitatory neural network.

To ensure that neuronal co-culture could respond to chemical or biological perturbation, tetrodotoxin (TTX), a sodium channel blocker well known to block synaptic transmission, was applied on neurons at a concentration of 10 nM. Prior to TTX exposure, basal recordings were performed and showed spontaneous activity in both cultures. We added TTX at different time points to test the fluidic isolation and modulation of neuronal networks in separate compartments of our microfluidic devices. TTX was specifically introduced into compartment Ch1 on D18 prior to the experimental procedures. On D19, TTX was subsequently administered to compartment Ch3. This timeline ensured sufficient recovery of baseline functional activity in neurons within Ch1, thereby enabling the effects to be distinctly localized and compartment specific (Fig. 3a). The effects of TTX on both glutamatergic neuron cultures were observed within minutes of its addition (Fig. 3b). At D18 and D19, raster plots showed a distinct reduction of detected spikes in the TTX-treated channel, and no change in functional activity in the opposite channel (Fig. 3c). To investigate the functional activity of neuronal networks, we assessed key electrophysiological parameters, including Mean Firing Rate (MFR), Weighted Mean Firing Rate (WMFR), and Synchrony Index, following tetrodotoxin (TTX) application and during recovery. These parameters were analysed in both channels and microchannels of the microfluidic device to differentiate activity patterns between somatic and axonal compartments. In channels, spontaneous activity was initially detected at D18 before TTX application. Following TTX treatment (D18 + TTX), a significant reduction in MFR was observed, confirming the expected inhibition of action potentials ($p < 0.05$). Upon TTX washout, partial recovery of MFR was detected at D19, with further recovery at D20, though still lower than baseline levels ($p < 0.05$) (Fig. 3d). A similar trend was observed in microchannels, where TTX significantly decreased activity, followed by progressive recovery (Fig. 3e). However, activity levels in microchannels were overall higher than in channels, suggesting differential sensitivity to TTX or differences in network connectivity. To refine our analysis, we calculated the WMFR, which represents functional activity on active electrodes. As shown in Fig. 3f (channels) and Fig. 3g (microchannels), a significant drop in WMFR was observed upon TTX application ($p < 0.05$), followed by a gradual restoration of activity at D19 and D20. The effect was particularly pronounced in microchannels, where activity remained more stable across replicates. Network synchrony, an indicator of functional connectivity, was assessed using the synchrony Index in both compartments (Fig. 3h for channels and Fig. 3i for microchannels). Prior to TTX application (D18), neuronal cultures exhibited stable synchrony patterns. TTX treatment induced a significant decrease in synchrony ($p < 0.05$), indicating effective silencing of coordinated neuronal firing. Notably, synchrony levels showed a progressive increase upon washout (D19 and

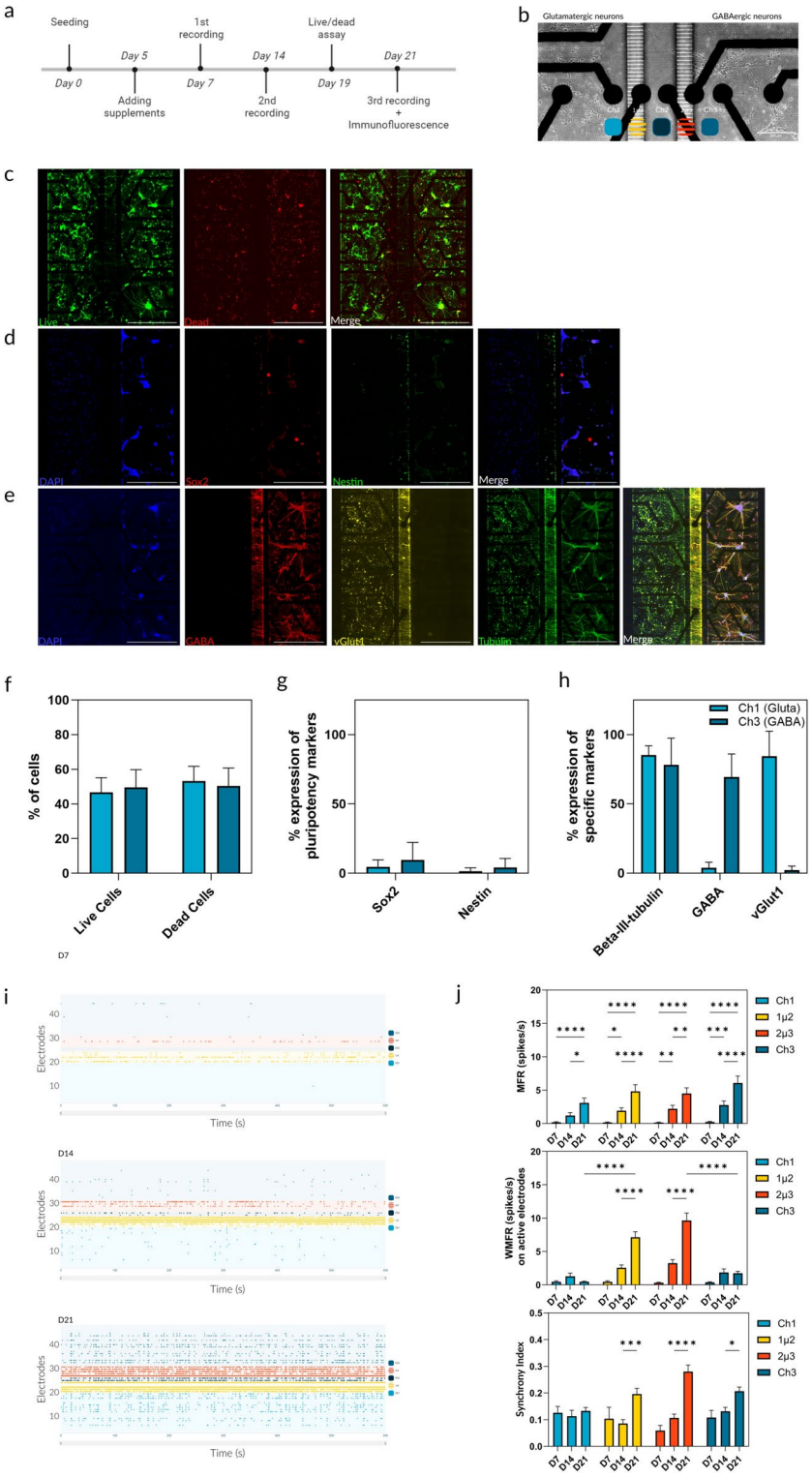

D20), with stronger recovery in microchannels than in channels. These results suggest that axonal activity within microchannels remains functionally interconnected despite transient synaptic silencing.

The effect of TTX was compared to vehicle and showed a significant difference in percentage of change MFR, WMFR and synchrony index to baseline (Supplementary Fig. S2). At D18, in Ch1 we observed a decrease of change to the baseline of MFR, WMFR and synchrony compared to vehicle. When TTX was added in Ch3, we observed a decrease of MFR, WMFR and synchrony compared to vehicle (Supplementary Fig. S2). We hypothesize that neurites from glutamatergic neurons in Ch1 extended into Ch3 through the 1µ2 and 2µ3 compartments and neurites from glutamatergic neurons in Ch3 extended into Ch1. This connectivity could explain the observed decreases in activity in the 2µ3 region when TTX was applied in Ch1, and in the 1µ2 region when Ch3 was treated with TTX (Fig. 3e,g,i). No significant difference in WMFR between D18 and D20 in channels nor microchannels was observed, showing the reversible effect of TTX on glutamatergic neurons

◂**Fig. 2**. Characterization of co-culture of human Glutamatergic and GABAergic neurons in microfluidic device. (**a**) Timeline of cell culture maintenance with milestones during culture. (**b**) Brightfield contrast pictures of human glutamatergic and GABAergic neurons seeded in Dualink MEA at day 16. (**c**) Fluorescent picture of Live/Dead assay in the co-culture. Live cells were stained in green, and dead cells in red. (**d, e**) Immunofluorescent pictures of respectively, pluripotency markers (d), and specific neuronal markers (e) for each cell type. Sox2 was marked in red and Nestin in green. B-III-tubulin was marked in green, vGlut1 in yellow, and GABA in red. In each immunofluorescent picture, DAPI was in blue. Scale bar represent 500 µm. (**f, g, h**) Graph bars showing the quantification in channel 1 and channel 3 of the Live/dead assay, pluripotency markers and neuronal specific markers, respectively. (**i**) Raster plots from electrophysiological recordings at day 7, day 14 and day 21, showing spikes in time per electrode, in each DuaLink compartment. (**j, k**) Bar graphs showing, respectively mean firing rate (MFR), weighted mean firing rate (WMFR) and Synchrony index at day 7, day 14, and day 21 measured in channels and microchannels. The data were analyzed using a two-way ANOVA to evaluate the effects of Ch1, Ch3, 1µ2 and 2µ3 and their interaction in time. Fisher's Least Significant Difference (LSD) test was used as a post-hoc analysis to compare specific group means. * p-value < 0.05, *** p-value < 0.001 and **** p-value < 0.001. Error bar = SD.

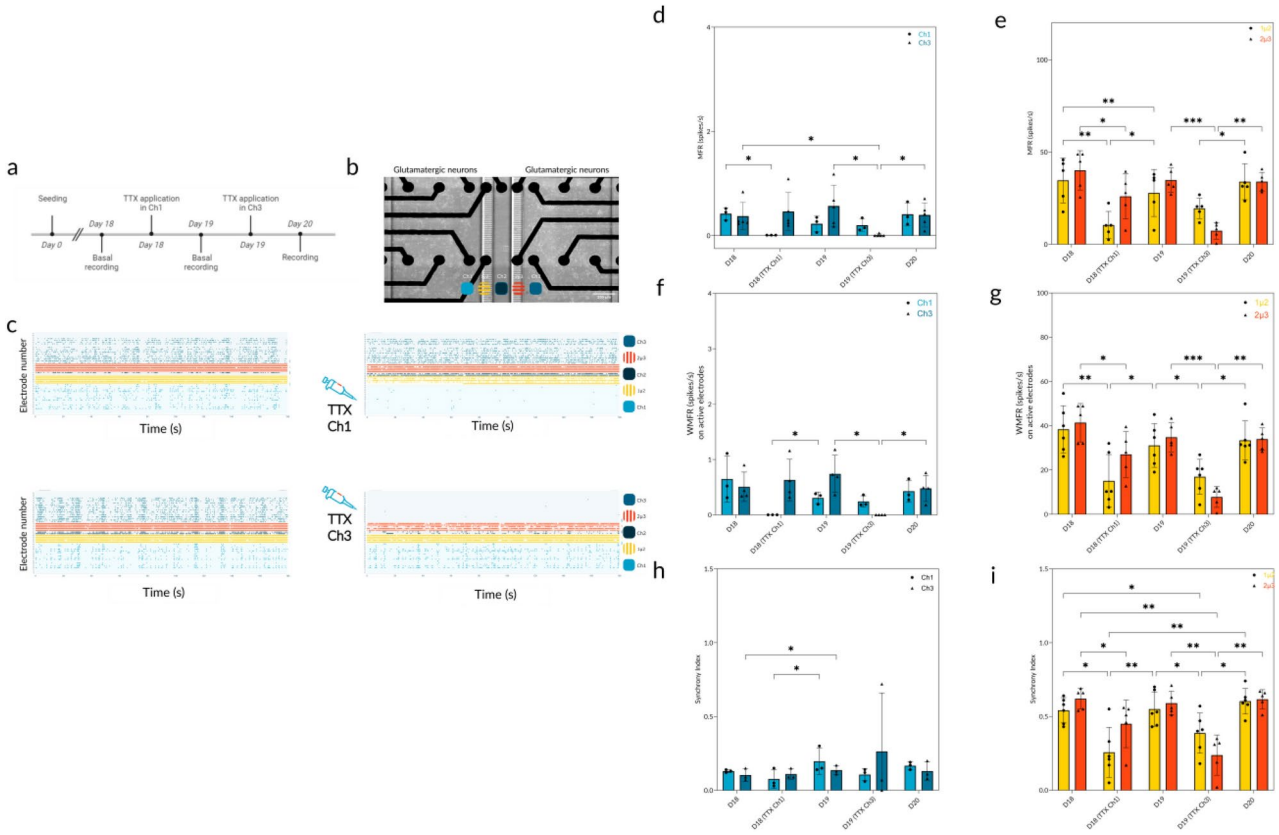

Fig. 3. Electrophysiological modulation of co-culture glutamatergic neurons with TTX. (**a**) Timeline of TTX exposure experiment steps. (**b**) Brightfield contrast pictures of compartmentalized glutamatergic neurons culture in Ch1 and Ch3, with the color legend of each compartment. (**c**) Raster plots before/after neuronal exposure of TTX in channel 1 or in channel 3. Bar graphs showing (**d,e**) MFR, (**f,g**) WMFR and (**h,i**) synchrony index in each step of TTX exposure in channels and in microchannels respectively. The data were analyzed using a two-way ANOVA to evaluate the effects of Ch1, Ch3, 1µ2 and 2µ3 and their interaction in time. Fisher's Least Significant Difference (LSD) test was used as a post-hoc analysis to compare specific group means. * p-value < 0.05, ** p-value < 0.01, *** p-value < 0.001 and **** p-value < 0.001. Error bar = SD. TTX: tetrodotoxin. MFR: mean firing rate, WMFR: weighted mean firing rate.

(Fig. 3d-i). Considering these results, we choose to only present microchannels (1µ2 and 2µ3) data for the following experiments. Furthermore, only the microfluidic devices that showed a successful response to TTX treatment, with evidenced by a significant decrease in neuronal activity, were selected for subsequent exposure to Aβ oligomers and CSF. This selection criterion ensured that the devices used in the Aβ and CSF experiments had functional networks capable of demonstrating the expected pharmacological effects.

Aβ oligomers peptides placed in a single compartment have an acute functional effect on the entire network

Aβ oligomers (AβO) were used at a concentration of 10 µM and added to Ch1 every 24 h without rinsing. This protocol was designed to mimic a chronic and accumulative exposure to AβO, reflecting the progressive peptide accumulation observed in the human brain. Baseline recordings were performed at D19 prior to the initial AβO application. Subsequent recordings were taken every 24 h before the reapplication of AβO to monitor the cumulative effects of chronic exposure. After 72 h of application, a final recording was performed, and the cells were fixed for further analysis. For comparison, a vehicle control was used, consisting of the solvent used to prepare AβO, and was applied following the same protocol. The composition of Aβ oligomers was assessed using Coomassie Blue staining combined with gel electrophoresis. This analysis provided an overview of the aggregation state and size distribution of the oligomers and monomeric present in the samples, confirming the presence of multiple forms (Supplementary Fig. S3). To assess the impact of chronic AβO exposure on neuronal activity, we recorded electrophysiological parameters following repeated AβO applications every 24 h. After 72 h, we observed a significant decrease in both MFR and WMFR in cultures treated in 1µ2 and 2µ3 ($p < 0.05$; Fig. 4b,c). In contrast, cultures treated with the vehicle control did not exhibit any significant changes in activity (Supplementary Fig. S4), confirming that the observed effects were specific to AβO treatment. A similar trend was observed in synchrony Index. After 72 h of AβO exposure, a significant decrease in synchrony was detected in the 1µ2 ($p < 0.05$; Fig. 4d), suggesting a disruption in coordinated network activity. To further refine our analysis, we normalized the data relative to the baseline to better capture activity changes over time. When expressed as a percentage of baseline, the decrease in MFR and WMFR was even more pronounced. Specifically, MFR showed a significant reduction in both 1µ2 and 2µ3 conditions ($p < 0.01$ *and* $p < 0.001$, respectively), while WMFR also significantly decreased for 1µ2 and 2µ3 ($p < 0.01$). Interestingly, for synchrony, a significant decrease was observed only in the 1µ2 condition ($p < 0.01$), whereas no significant reduction was detected for 2µ3. Moreover, we performed the same experiments using two additional concentrations: 1 µM and 5 µM. We observed a similar trend toward decreased activity, particularly in the 5 µM condition, where the reduction in firing rates and synchrony was more pronounced. However, the results were less conclusive, as the evolution of activity over time appeared to be less progressive compared to the 1µ2 and 2µ3 conditions (Supplementary Fig. S5). These results highlight a progressive decline in neuronal activity following chronic AβO exposure, with both spontaneous firing and network synchrony being differentially affected depending on the AβO concentration. To further refine our analysis, we normalized the data by subtracting the vehicle control from the functional activity at each time point. The difference index, expressed as the subtraction of the mean vehicle value from each individual functional activity measurement, was negative for MFR, WMFR, and synchrony, indicating a reduction in neuronal activity following AβO exposure. Additionally, we observed a significant difference in this index between 24 and 72 h of exposure for MFR and WMFR ($p < 0.05$), suggesting a progressive decline in activity over time. However, no significant difference was detected for synchrony (Fig. 4h-j).

Effect of non-neurodegenerative and AD patients' CSF exposure in neuronal networks

Prior to experiments, CSF of NN and Alzheimer's patients were analysed, and biomarkers such as Aβ1–42, Tau total and p- 281-tau were measured. Levels of Aβ1–42 tended to be lower in NN patients compared to AD's patients. There was no correlation between the tau level in CSF's patients and the presence of the disease (Supplementary Table S1). Following the experimental plan used for the Aβ experiments, CSF from NN (n = 2) and Alzheimer's patients (n = 3) were chronically added on glutamatergic neurons in Ch1, at D19 every 24 h during 72 h (Fig. 5a). Initial exposure of AD CSF tended to increase neuronal activity at 24 h in 1µ2 ($p < 0.01$ for A1 and A3) and in 2µ3 ($p < 0.05$ for A1 and $p < 0.01$ for A2) (Fig. 5b, c, d). From 24 to 72 h, no significant change of activity was observed. Non neurodegenerative CSF from H1 patient didn't change activity overtime (Fig. 5e). Unexpectedly, the CSF of H2 patient tend to improve neuronal activity in 2µ3 compartment after 24 h and 72 h of exposure (Fig. 5f). The same experiment was performed with fresh media as a control. As expected because of the media composition, WMFR improved overtime in 1µ2 at 24 h and 48 h ($p < 0.05$ and $p < 0.01$) and in 2µ3 at 48 h and 72 h ($p < 0.05$ and $p < 0.01$) (Fig. 5g).

When normalizing to baseline (Fig. 5h–m), we observed that WMFR remained relatively stable over time in both AD and non-neurodegenerative CSF conditions, with no significant decrease at T + 24 h, T + 48 h, or T + 72 h. In contrast, control media (Fig. m) showed a significant increase in WMFR at T + 48 h and T + 72 h in 1µ2 (respectively $p < 0.0001$ and $p < 0.01$,), suggesting that normal culture conditions with media composed of BrainPhys, promote spontaneous activity enhancement over time. To better isolate the effects of CSF itself, we subtracted the control media response from each CSF-treated condition (Fig. n–o). In AD-CSF conditions (Fig. n), the difference index remained close to zero with a trend to a positive index, indicating that these CSF samples did not significantly modulate neuronal activity beyond the intrinsic culture evolution. However, in non-neurodegenerative CSF conditions (Fig. o), we observed a significant difference in WMFR at multiple time points (T + 24 h, T + 48 h, T + 72 h, $p < 0.05$ to $p < 0.0001$), suggesting a stronger modulatory effect of non-neurodegenerative CSF on neuronal activity compared to AD-CSF. Moreover, we observed a significant difference index between 1µ2 and 2µ3 at T + 48 h and T + 72 h. Interestingly, while neurons exposed to control media exhibited a progressive increase in WMFR, this trend was not observed in AD-CSF, possibly reflecting an impaired regulatory effect of AD-related factors present in the CSF. These results indicate that CSF from non-neurodegenerative individuals may exert a stronger influence on neuronal activity over time, while CSF from AD patients does not significantly alter the functional activity of neurons compared to control conditions. The results for MFR and synchrony index are also presented in the supplementary data (Supplementary Fig. S6), where we observed similar trends to those seen with WMFR. Specifically, in non-neurodegenerative CSF conditions, both MFR and synchrony index showed significant changes over time (T + 24 h, T + 48 h, T + 72 h), supporting the stronger modulatory effect on neuronal activity. In contrast, no significant modulation was

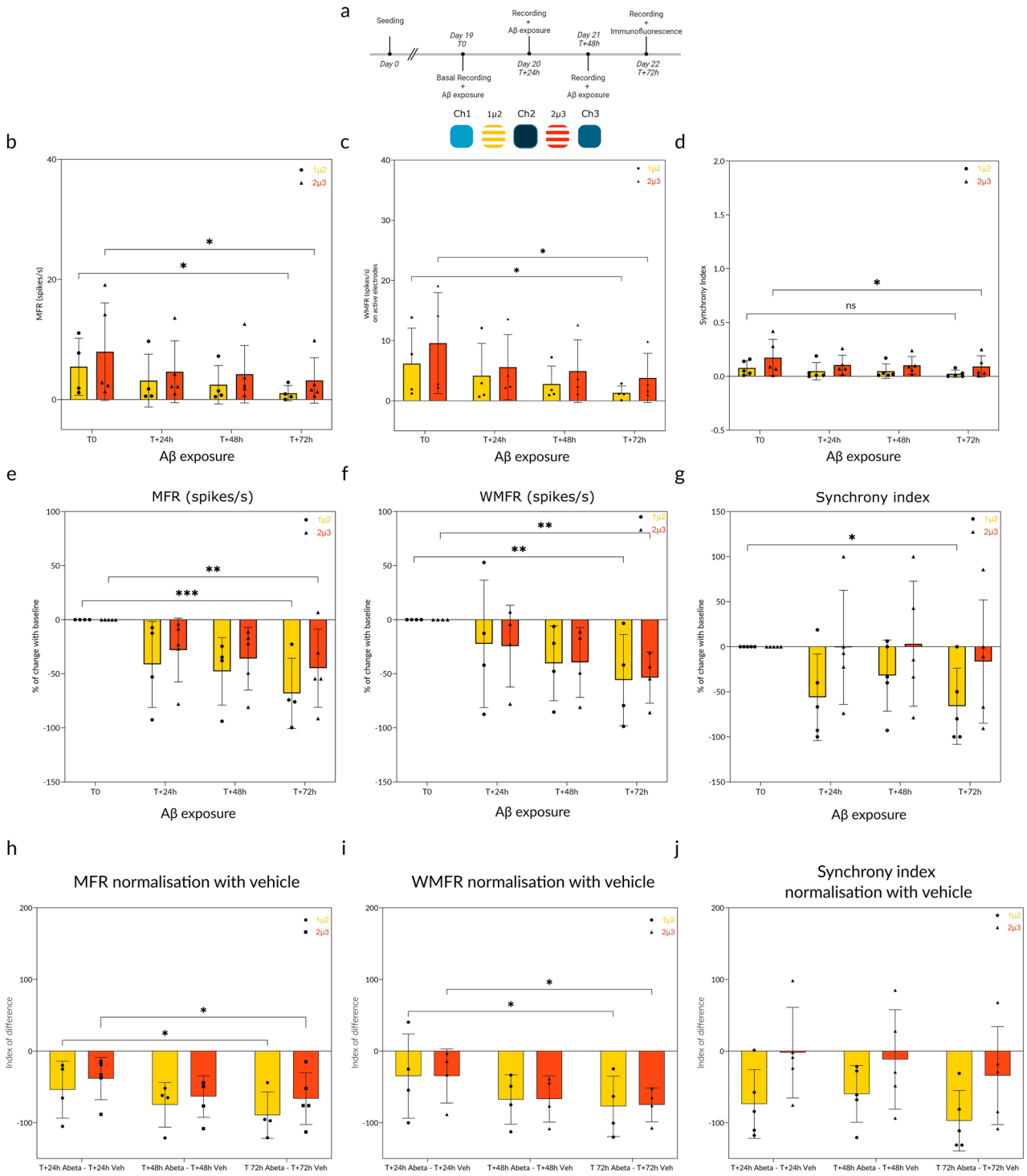

Fig. 4. Electrophysiological effect of Aβ exposure on co-culture glutamatergic neurons. (**a**) Timeline of Aβ exposure experiment steps. (**b**) Bar graph of WMFR in microchannels of chronic Aβ exposure in time respectively. The data were analyzed using a two-way ANOVA to evaluate the effects of 1μ2 and 2μ3 and their interaction in time. Fisher's Least Significant Difference (LSD) test was used as a post-hoc analysis to compare specific group means. * p-value < 0.05, ** p-value < 0.01, *** p-value < 0.001 and **** p-value < 0.001. Error bar = SD. MFR: Mean firing rate, WMFR: weighted mean firing rate.

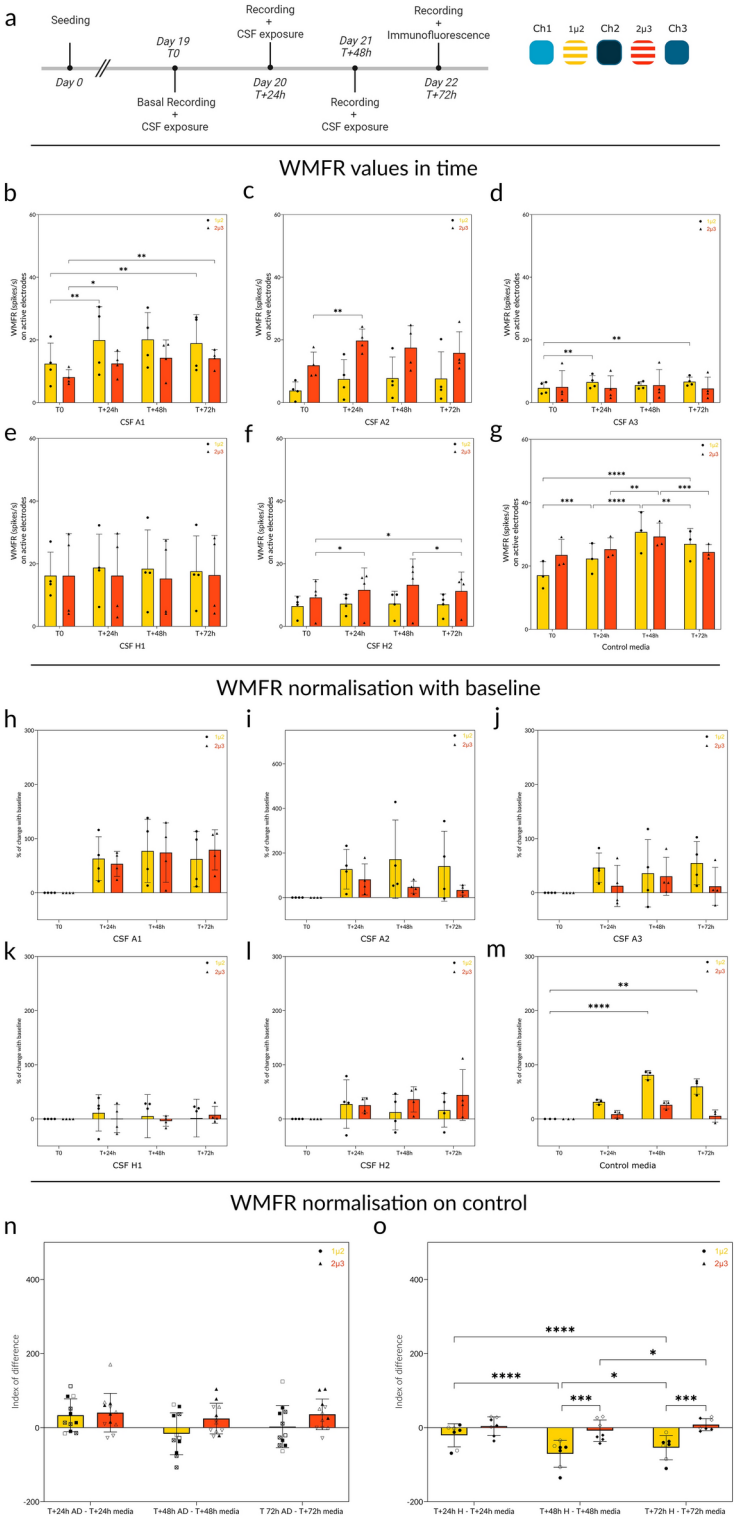

detected in AD-CSF conditions for either MFR or synchrony index, further corroborating the lack of significant alteration in neuronal activity in response to AD-related factors. These findings provide additional evidence for the differential effects of CSF from non-neurodegenerative and AD individuals on neuronal behavior.

These initial results did not allow us to clearly distinguish patient samples based on their effects on neuronal activity. To further investigate potential differences, we performed correlation analyses to explore relationships between electrophysiological parameters. Additionally, we generated a scatter plot to visualize the interaction between two key electrophysiological metrics, plotting the different experimental conditions over time. All recorded electrophysiological metrics were included in the analysis. The correlation matrix revealed no strong correlation between WMFR and the synchrony index for AD patients (Fig. 6a). To refine the analysis, we set a correlation threshold of 0.7 to identify metrics with strong relationships. Metrics exceeding this threshold were excluded to prevent redundancy and ensure a balanced analysis. This filtering allowed us to focus on a subset of

◂**Fig. 5**. Electrophysiological effects of Alzheimer's disease (AD) and non-neurodegenerative (NN) patient CSF exposure on co-cultured glutamatergic neurons. (**a**) Timeline of the CSF exposure experiment. (**b–d**) Bar graphs showing microchannel weighted mean firing rate (WMFR) over time following chronic exposure to CSF from three anonymous Alzheimer's patients (A1, A2, and A3). (**e–f**) Bar graphs showing WMFR over time following chronic exposure to CSF from two anonymous non neurodegenerative patients (H1 and H2). (**g**) Bar graph showing WMFR over time following chronic exposure to control media (BrainPhys). (h–m) WMFR normalization relative to baseline for each condition: (**h–j**) AD patients (A1, A2, A3), (**k–l**) NN patients (H1, H2), and (**m**) control media. (**n**) WMFR normalization relative to control media for Alzheimer's patient CSF conditions. (**o**) WMFR normalization relative to control media for non-neurodegenerative patient CSF conditions. The data were analyzed using a two-way ANOVA to evaluate the effects of 1µ2 and 2µ3 and their interaction in time. Fisher's Least Significant Difference (LSD) test was used as a post-hoc analysis to compare specific group means. * p-value < 0.05, ** < 0.01, *** < 0.01 and **** < 0.0001. Error bar = SD. CSF: cerebrospinal fluid. MFR: mean firing rate, WMFR : weighted mean firing rate.

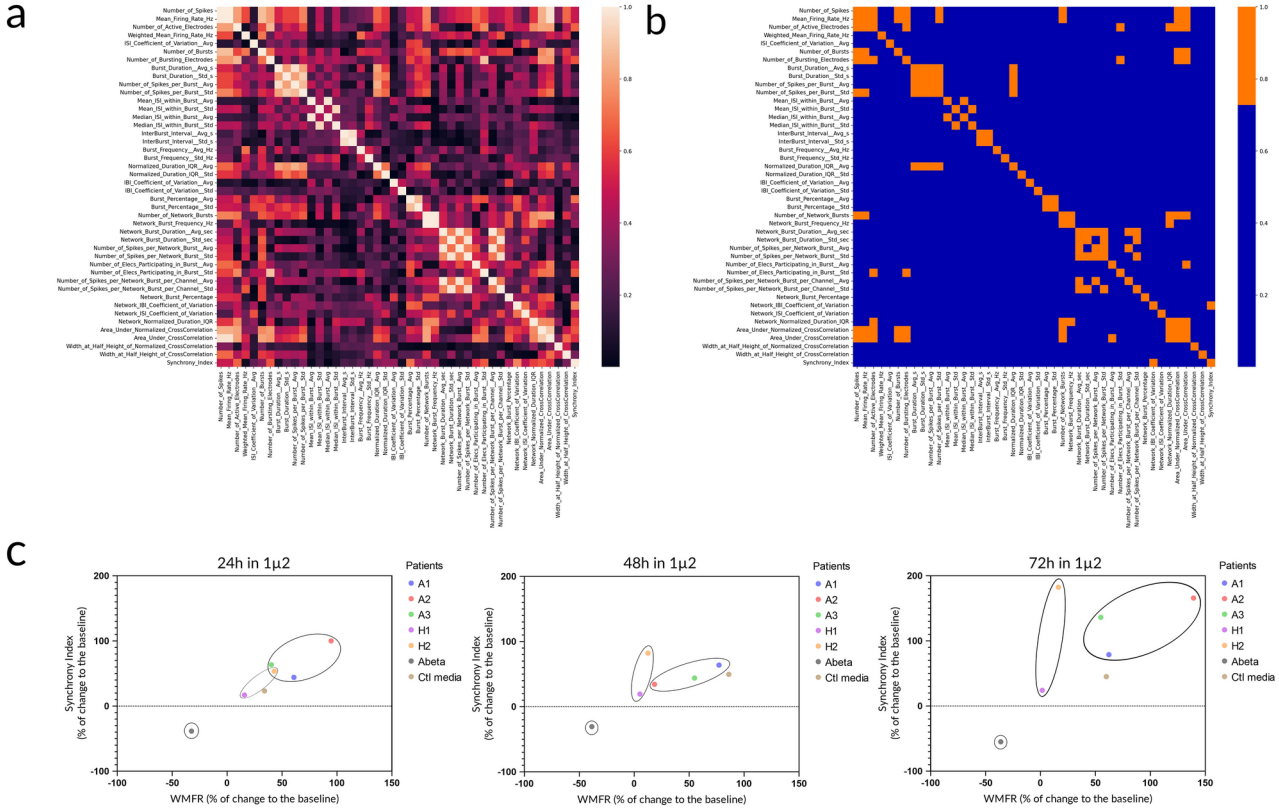

Fig. 6. Electrophysiological analysis of CSF from AD and non-neurodegenerative patients' exposure on glutamatergic neurons. (**a**) Correlation matrix of normalized dataset from all electrophysiological metrics. Each cells represents the Pearson correlation coefficient between pairs of metrics. Correlation coefficients range from 0 to 1. (**b**) An arbitrary threshold of 0.7 was applied to differentiate strong (in orange) and weak (in blue) correlations between metrics. (**c**) Scatter plots of synchrony index and WMFR at 24 h, 48 h and 72 h after experiments in 1µ2 compartment.

metrics (highlighted in blue) (Fig. 6b), which were subsequently used to generate scatter plots illustrating the interaction between two of those weakly correlated metrics. These scatter plots enabled us to identify potential trends and interactions in the electrophysiological responses of neurons. Scatter plots, showing the % of change to the baseline after 24 h, 48 h and 72 h of exposure in 1µ2 microfluidic compartments were created. At the 24 h the scatter plot shows a relatively mixed distribution of patient groups. Data points may be closely clustered, indicating that at this early stage, the differences between the patient groups are not yet pronounced. At 48 h, the scatter plot begins to show a tendency for patient groups to differentiate. Data points may start to spread out, with some groups forming distinct clusters. At 72 h, the scatter plot suggests a trend toward a more pronounced separation and expansion of patient groups. The clusters representing the different groups appear to show reduced overlap, indicating a potential differentiation based on the measured variables. This trend hints that each group may exhibit distinct profiles or responses, though further analysis would be required to confirm these observations (Fig. 6c). We observed a trend toward separation, suggesting the emergence of distinct condition-dependent clusters. However, these findings should be interpreted with caution, as the sample size

(n = 3 for AD patients and n = 2 for NN patients) remains low, limiting the statistical power and generalizability of the observed trends. Further analyses with larger datasets are required to confirm these preliminary insights.

Discussion

In this study, we investigated the effect, AβO and AD patients' CSF on functional activity of a compartmentalized culture of glutamatergic neurons. Prior to exposing neurons to AβO and CSF, we ensured that glutamatergic neurons were fully differentiated and capable of responding to chemical stimuli (TTX).

A key observation in these analyses is the differential sensitivity of channels and microchannels in detecting electrophysiological activity. While channels record from neuronal cell bodies and proximal dendrites, their positioning over electrodes is less constrained, potentially reducing the detection of action potentials. In contrast, microchannels are entirely encompassed by electrodes, ensuring that isolated axons remain within the recording sites, thereby improving signal detection. This explains why microchannels display higher reproducibility and more robust activity levels compared to channels, where spontaneous firing was often below the inclusion threshold (< 0.1 spikes/s). Consequently, for conditions where channel activity was extremely low (e.g., following Aβ application), analyses were focused on microchannels to ensure reliable data interpretation.

These findings highlight the importance of considering spatial compartmentalization when interpreting electrophysiological data and validate the experimental approach for assessing neuronal activity under different perturbations. The control media used in these experiments contained BrainPhys, a neuronal culture medium optimized to support synaptic activity and network maturation[25]. This phenomenon, well documented, can be explained by the microchannels architecture[26,27]. Indeed, the confined compartments increase electrode impedance due to the electrical resistance of the microchannel, leading to an increase in spike amplitude thus enhancing the signal–noise ratio[28]. Our results demonstrate the inhibitory effect of TTX[21,29] on glutamatergic neurons activity, in channels and microchannels, as evidence by the decrease of WMFR in TTX-treated channel and axonal compartments. To assess the fluidic isolation within the microfluidic system, we conducted TTX experiments by selectively applying the treatment to one compartment. The results showed a localized reduction in neuronal activity within the treated area, while the activity in the untreated compartment remained unchanged. This suggests that fluid mixing between compartments was minimal, allowing the treated and untreated neuronal populations to remain functionally distinct. While these findings support the effectiveness of the microfluidic system in maintaining fluidic isolation, further validations could help refine the system's precision.

This allowed us to perform AβO exposure on glutamatergic neurons seeded in Ch1 to observe the effect of the neuronal network. We observed exposing human glutamatergic neurons to 10 µM AβO resulted in a significant decrease in functional activity after 72 h of exposure. However, the used concentration was a thousand times higher than Aβ1–42 measured in human CSF from NN and AD patients[30](Supplementary Table S1). Tests using 1 µM and 5 µM of AβO were also conducted but did not show an effect on functional activity (Supplementary Fig. S5). Some research showed that AβO had an effect on neurons and synaptic communication at lower concentration as 1, 2 or 5 µM in conventional cell culture as a Petri dish[31–34]. Several studies have investigated the synaptic effect of Aβ peptides in microfluidic devices made of PDMS, to evaluate the viability[35], the synaptotoxicity[36] and the impact on the functional activity of neuronal cultures[2,37]. Lefebvre et al.[37], in 2024, used an asymmetric microfluidic device allowing to isolate synapses from neuronal culture. They investigated the effect of Aβ on synaptic functional activity in a directional neuronal network showing that applying Aβ to the synapses for 48 h significantly reduced inter-compartments connectivity without causing a substantial change in neuronal activity within the presynaptic or postsynaptic chambers[37]. In our study, we used a symmetric microfluidic device to recreate a bidirectional neuronal network, allowing us to observe the effects of Aβ and CSF in glutamatergic neurons (Ch1 and 1µ2, Fig. 1d) and assess the impact and the potential response of both cultures (Ch3 and 2µ3, Fig. 1d) allowing to mimic the natural interactions that occur in the brain, where neurons communicate in both directions[38].

Exposure of glutamatergic neurons to AD patients' CSF led to an increase in spike rate on active electrodes within 24 h. While cytotoxicity was not directly tested, this observation suggests that, despite the addition of CSF, the neurons remained present and exhibited functional activity higher than baseline levels. As previously reported by Yaka et al., CSF of AD patients showed no cytotoxicity on neuron-like cells as PC12[39]. In contrast, some publications related the adverse effect of CSF from AD on rodent cell viability and neurotoxic effects[40,41]. It is known that CSF from neurodegenerative disease could affect in vitro glial cells as reported by Schiess et al., with Parkinson's disease patients' CSF exposure[42]. It could be explained by the fact that CSF has a cytotoxic effect on in primary cells[40,41]rather than immortalized cell lines[39]. In our study, human glutamatergic neurons iPSCs-derived were composed of about 85% of neurons in our microfluidic technology explaining that we didn't show the same effect of CSF on our culture (Fig. 2h) than on primary cells[40,41].

Several studies used NN and artificial CSF on neural stem cells and have reported that they could promote stem cells proliferation capacity[43], glial differentiation[43–45]and neuronal circuit maturation[46]. CSF could have a beneficial effect on iPSCs-derived human neurons and then an increase of functional activity, as we have shown with CSF from NN patients (H1 and H2).

In contrast we expected to observe a cytotoxic effect with applying diseased CSF directly on neurons. Several studies reported that exposing CSF from patient suffering from amyotrophic lateral sclerosis on rodent cells and iPSC motor neurons[47,48]or Parkinson's disease on dopaminergic neurons[49–51] had a cytotoxic effect.

Our study revealed an increase in functional activity following exposure to CSF from AD patients. This aligns with findings from Görtz et al.[52], who observed a similar spike rate increase in rodent cortical cultures exposed to AD-CSF. However, their study also showed a decrease in activity when comparing AD-CSF to CSF from mild cognitive impairment (MCI) patients, an earlier disease stage. Both studies used BrainPhys neuronal media, known for its excitatory effects, which may have contributed to the progressive increase in activity over time in our control condition (Fig. 5g). Baseline-normalized WMFR graphs confirmed this trend, with

significant activity increases in control media (Fig. 5m, $p < 0.01$, $p < 0.0001$ at T + 72 h). This could be expected, as BrainPhys provides essential substrates that enhance neuronal excitability and synaptic function. However, neurons exposed to AD-CSF did not show this progressive increase, suggesting potential inhibitory effects from pathological CSF components, such as altered ion composition, inflammatory mediators, or toxic protein aggregates.

To refine our electrophysiological analysis, we performed correlation analyses between WMFR and synchrony index, visualized in scatter plots across 24 h, 48 h, and 72 h (Fig. 6). Over time, we observed a gradual divergence in patient groups, with clearer separation at 72 h, suggesting distinct functional effects of CSF exposure. However, due to the small sample size (AD: n = 3, non-neurodegenerative: n = 2), these findings should be interpreted with caution. Since the study by Görtz et al.[52], few studies have investigated AD-CSF effects on neuronal activity using MEA technology, likely due to the complex and poorly understood nature of CSF composition. In 2019, Koch et al. (Koch et al., 2019)14 demonstrated the potential of MEA assays by showing that CSF from autoimmune encephalitis (AE) patients could significantly reduce neuronal activity, highlighting the utility of such approaches.

CSF is a dynamic and complex biological fluid containing proteins, metabolites, electrolytes, and signalling molecules, including pro-inflammatory and redox factors, making its study challenging[53]. Traditional research has focused on identifying biomarker ratios, but here, we propose a novel strategy using a microfluidic platform with human neurons as biosensors. This system enables the targeted exposure of one neuronal population to CSF while monitoring remote network responses, effectively translating biochemical changes into functional readouts. This approach offers a more integrated perspective on CSF effects, providing a complementary tool for studying neurological diseases and their potential diagnostic applications.

Investigating the effects of CSF in vitro remains challenging due to its complex composition and variability. However, our approach using a microfluidic platform combined with MEA recordings provides valuable insights into how CSF from different patient groups influences neuronal activity. While we observed trends suggesting differences between AD and non-neurodegenerative CSF samples, further refinements are needed to improve the sensitivity and robustness of this device. Recently, microfluidic technology has been used to investigate biological fluids allowing to develop new tools for AD diagnosis and biomarkers detection[54–56]. As we have shown, microfluidic platform coupled with MEA provides a relevant tool to investigate the functional effect of a perturbation of neuronal culture. One possible improvement of our device could be the use of oriented unidirectional co-cultures to better control and analyze synaptic connectivity and signal propagation. Technologies such as axon diodes or arches[57,58]could help ensure selective axonal crossing, allowing for more precise investigations of network activity. Additionally, asymmetric microfluidic devices could facilitate the isolation of synapses as well as unidirectional compartmentalized co-cultures, providing a more detailed understanding of how neuronal communication is altered under different conditions[27,57,59,60]. Further developments could also include co-cultures combining excitatory (glutamatergic) and inhibitory (GABAergic) neurons to explore how CSF influences the balance of excitatory and inhibitory signaling. Since disruptions in this balance are a hallmark of many neurological disorders, this approach could offer additional insights into disease-related network dysfunction[61–63]. While our current findings indicate trends in network activity changes in response to CSF exposure, increasing the number of samples and refining the experimental model will be necessary to strengthen the interpretability of these results.

Our study highlights the potential of using electrophysiological metrics to analyse functional changes over time in neurons cultured within compartmentalized microfluidic platforms. While the scatter plot analysis of two key metrics provided initial insights into the relationship between conditions (three Alzheimer's disease patients and two non-neurodegenerative), this represents a proof-of-concept demonstration rather than a definitive diagnostic tool. The ability to distinguish between experimental conditions based on these metrics validates the feasibility of this approach but underscores the need for further refinement and expansion.

Future work should involve an in-depth exploration of the full array of electrophysiological metrics available through the tools used in this study. Dozens of additional metrics could enhance the sensitivity and specificity of the detection platform, potentially uncovering subtle differences between disease states. Visualization techniques, such as scatter plots and cross-correlation graphs, can further clarify relationships between metrics and identify patterns or anomalies that might be overlooked in single-metric analyses. Automating these analyses would be essential to improve the precision and reproducibility of the detection system, particularly as the dataset grows.

Increasing the number of patient samples is also critical for validating and enhancing the sensitivity of the platform. A larger, more diverse cohort would enable robust statistical analyses and improve the reliability of the conclusions, paving the way for broader applicability across neurodegenerative diseases.

This study supports the concept of using neurons as sensors within a compartmentalized microfluidic platform for differential diagnosis of neurological disorders. By introducing patient-derived CSF into one compartment, we demonstrated the potential to monitor changes in neuronal activity across the network and observe condition-specific patterns. This innovative approach could facilitate the early and precise diagnosis of neurodegenerative diseases and guide patient stratification for clinical trials. Furthermore, the platform has the potential to advance personalized therapeutic strategies by assessing how individual patient samples influence neural networks, ultimately contributing to the development of novel treatments.

Materials and methods

High throughput microfluidic devices coupled with microelectrode array (MEA)

Microfluidic devices with three compartments including two symmetrical culture chambers and linked with microchannels were fabricated using Polydimethylsiloxane (PDMS) and conventional photolithography technique as previously described in Honegger et al.[64], called DuaLink MEA (NBP_TLN-AX, NETRI, Lyon).

Microfluidic devices were bonded with oxygen plasma in an Axion Biosystem custom-made sheets composed of MEA. MEA devices were filled in with 70% ethanol and three washes of distilled water before coating.

Human cells

Human-induced pluripotent stem cell-derived cortical glutamatergic neurons (BrainXell, BX- 0300, Madisson, WI, USA) and GABAergic neurons (BrainXell, BX- 0400, Madisson, WI, USA) were purchased. Human-derived materials were preserved and handled with the approval and under the guidelines of French legislation. The accreditation number related to the use of human materials is DC- 2020–4203. Microfluidic devices were previously coated with Poly-D-Lysine (PDL) (0.05 mg/mL) overnight at 37 ∘C under 5% CO2. Glutamatergic and GABAergic neurons were seeded by placing 3 µL of a 1×10^7 cells/mL neuron suspension in the inlet reservoir of targeted channels, depending on experimental conditions at a density of 1500 cells/mm^2. Cell culture media was composed of DMEM/F12 medium (Sigma, D8437), Neurobasal medium (Thermofisher, 21,103,049), NeuroCult SM1 Supplement (StemCell 05,711),N2 Supplement-A (StemCell, 07,152), GlutaMAX (Sigma, G8541), BDNF (Preprotech, 450–02), GDNF (Preprotech, 450–10), TGF-β1 (Preprotech, 100 - 21 C), seeding supplement for glutamatergic neurons (BrainXell), Supplement K (BrainXell), Geltrex (Thermofisher, A1413202), and BrainPhys (StemCell, 05,790) (Stemcell Technologies, Canada, #05,790), known a neuronal activity improvement, as providers recommendations. Fresh media were replaced every 2 to 3 days with provider media, as previously described[65]. Neurons were cultured for up to 21 days under a controlled environment (37 °C and 5% CO2). Human-derived materials were preserved and handled with the approval and under the guidelines of French legislation. The accreditation number related to the use of human materials is DC- 2020–4203.

TTX preparation and exposure

Tetrodotoxin (TTX), a potent and specific blocker of voltage-gated sodium channels has been purchased at Laxotxan (L- 8502, Laxotan, Velcen, France) and was prepared at a stock solution of 10 mM in sterile phosphate-buffered saline (PBS) and stocked at − 20 °C. Neurons in culture were exposed to a working solution of TTX diluted in fresh culture media at a concentration of 10 nM. Neuronal cultures were exposed to TTX for a few minutes without washout. Real-time recordings were taken to record the immediate effects of neuronal firing. Recordings were performed 24 h post-TTX exposure on culture to evaluate the recovery of neuronal activity.

Beta amyloid oligomers (AβO) preparation

AβO were obtained from Etap Lab (Nantes, France). Oligomers were diluted to the targeted concentration and mixed with cell culture media for direct application. As a control, vehicle from AβO preparation buffer and cell culture media have been used. Human amyloid beta 1–42 monomers were obtained from Bachem (Germany). Oligomers were prepared as described previously (Dahlgren et al., 2002). Briefly, amyloid beta peptide was dissolved to 1 mM in 100% hexafluoroisopropanol (HFIP). HFIP was removed under a nitrogen stream, then peptide was resuspended in DMSO to 5 mM. F- 12 (without phenol red) culture media was added to bring the peptide to a final concentration of 500 µM, and the peptide was incubated at 22 °C for 18 h. Oligomers were then aliquoted and stored frozen at − 80 °C until use.

Coomassie Staining and Gel Electrophoresis

To assess the aggregation state and size distribution of Aβ oligomers, the samples were analyzed using Coomassie Brilliant Blue staining in conjunction with sodium dodecyl sulfate–polyacrylamide gel electrophoresis (SDS-PAGE). Briefly, 10 µg of Aβ oligomers were loaded onto a 4–12% gradient SDS-PAGE gel and electrophoresed at 120 V for 90 min. After electrophoresis, the gel was stained with Coomassie Brilliant Blue R- 250 for 1 h, followed by destaining in a solution of 40% methanol and 10% acetic acid until the background was clear. Protein bands were visualized to assess the size distribution and aggregation profile of Aβ oligomers.

CSF from patients' collection and analysis

CSF collection, sampling and storage were performed using a standard procedure according to the international consensus[66]. The concentrations of Aβ1–42, t-Tau, pTau181 and Aβ1–40 were measured routinely using Lumipulse G 600II (Fujirebio) in the neurochemistry laboratory (Hospices Civils de Lyon, Groupement Hospitalier Est, Lyon, France) (Supplementary Table S1). The cut-off values defined by the laboratory, considering a positive AD CSF biomarker profile were t-Tau ≥ 400 ng/L, pTau181 ≥ 60 ng/L, and Aβ1–42 ≤ 550 ng/L and/or a Aβ1–42/Aβ1–40 ratio < 0,055 (Molinuevo et al., 2014). All the assays were performed in the laboratory according to ISO 15,189:2012 standard (n°8–3442 rev.28). Patients or their relatives gave their written consent to save CSF for research purposes. Samples were stored in a biobank with authorization from the French Ministry of Health (Declaration number DC- 2008–304). Prior to use, CSF was diluted to 10% v/v in cell culture media before addition to culture media. As control, fresh culture media was added on neurons.

Immunofluorescence

Cultures were fixed in 4% paraformaldehyde (PFA) for 30 min at room temperature, as previously described[65]. Briefly, cells were washed three times with PBS and permeabilized for 10 min with 0.1% Triton-X100, followed by 30 min with 3% BSA. Primary antibodies: mouse anti-Nestin (1:500 (1 µg/mL), ThermoFisher, 14–9843 - 82), rabbit anti-Sox2 (1:500 (2 µg/mL), Merck, AB5603), guinea pig anti-vGlut1 (1:100 (5 µg/mL), Synaptic Systems, 135,304), rabbit anti-GABA (1:50 (5 µg/mL), Sigma-Aldrich, A2052), rabbit anti-MAP2 (1:500 (1 µg/mL), Abcam, ab96378), and mouse anti-βIII-tubulin (1:200 (5 µg/mL), ThermoFisher, MA1 - 118) were added, and the devices were incubated overnight at 4 °C. The cells were rinsed three times with PBS and further incubated with the corresponding secondary antibodies : Alexa Fluor 488 goat anti-mouse IgG (1:1000, Abcam, ab150061),

Alexa Fluor 647 donkey anti-rabbit IgG (1:1000, Abcam, ab150075), Alexa Fluor 647 goat anti-guinea pig IgG (1:1000, Abcam, ab150187), Alexa Fluor 555 donkey anti-mouse IgG (1:1000, Abcam, ab150110) and Alexa Fluor 488 donkey anti-rabbit IgG (1:1000, Abcam, ab150061, for 2 h at room temperature in the dark. For the quantification of antibodies, the percentage of the positive cells was quantified compared with DAPI (Sigma-Aldrich, D8417) positive using a homemade macro in Image J (v1.53q). Images were acquired with an inverted epifluorescence microscope, the AxioObserver 7 (Zeiss), with a CMOS camera.

Live/dead assay

Cell viability assessment was performed as previously described 65,656,565. Briefly, cells were incubated with the LIVE/DEAD™ Viability/Cytotoxicity Kit (L3224, Thermo Fisher Scientific Inc., USA), for 30 min at room temperature and were imaged without washing.

Image analysis

All microscope pictures were treated with NETRI's proprietary software developed with ImageJ (National Institutes of Health, Bethesda, MD, USA) (v1.53q) allowing to quantify the number of positive cells stained with fluorescence. To quantify the percentage of positive cells, fluorescence intensity thresholds were established for each marker. First, the software was"trained"by the user, who manually defined the threshold fluorescence intensity that differentiated positive cells from negative ones based on representative images. This threshold was then applied to the entire dataset. After setting the threshold, the software identified and counted cells positive for the fluorescent marker of interest. Simultaneously, nuclei were identified and counted using DAPI staining as a reference for the total cell population. The percentage of positive cells was calculated as the ratio of fluorescence-positive cells to the total number of DAPI-stained nuclei.

Electrophysiological recordings and analysis

Electrophysiological recordings were performed with commercial hardware and software by Axion Biosystems (Axion Biosystems, Atlanta, GA). MEA recordings were performed using the Maestro Pro MEA system (Axion Biosystems). Baseline neuronal activity was recorded for 10 min before any treatment use as a control baseline of activity. The recorded data were analyzed using AxIS Navigator software (Axion Biosystems) and NETRI's proprietary software NETRI UpLink, which facilitated the extraction of electrophysiological metrics such as MFR and raster plots, WMFR and synchrony index, for each compartment (Fig. 1f).

The threshold for spike detection was set at 6× the standard deviation of the noise level of the root mean square (RMS), which was determined from the initial segment of the recording without evident neuronal activity. This method ensured reliable discrimination of true neuronal spikes from background noise.

The mean firing rate (MFR) is the number of spikes per second from each channel and was calculated on all the electrodes divided by recording time, while the weighted mean firing rate (WMFR) corresponds to the number of spikes per second from each channel and was calculated only on the signal detected on the active electrode. An active electrode has been considered when the electrode detects at least 0.1 spikes/s. Recordings with an activity less than 0.1 spikes per second (spikes/s) at day 18 (D18) for TTX experiments and at day 20 (D20) for other tests (including Aβ and CSF treatments) were excluded from the analyses.

The values of MFR, WMFR, and synchrony index were expressed in raw form, as well as normalized relative to baseline activity (in % change). This normalization was performed by calculating the percentage change relative to the baseline activity observed during the initial control period (before any treatment). Additionally, the values were also normalized relative to the vehicle or culture media by subtracting the average vehicle values at each recorded condition point.

To analyse the relationships between electrophysiological metrics, we constructed a correlation matrix to evaluate the interaction between different metrics. All electrophysiological metrics recorded from the microfluidic MEA devices were included in this analysis. The correlation matrix was generated by calculating Pearson correlation coefficients between each pair of metrics across all experimental conditions. A threshold of 0.7 was used to identify pairs of metrics with strong correlations. Metrics that exceeded this threshold were excluded from subsequent analysis to avoid redundancy and overemphasis on closely related variables.

Data analysis

Data were analyzed using GraphPad Prism version 10.2.2 (GraphPad Software, San Diego, CA, USA). All experimental results are presented as mean ± standard deviation (SD) or Standard Error of the Mean (SEM) for $n > 10$. Data points from individual experiments are shown alongside the mean values to illustrate variability. For comparisons between multiple groups (days of experiment), a two-way analysis of variance (ANOVA) was performed. Post-hoc multiple comparison tests were conducted to identify significant differences between groups using Tukey's test or Fisher's LSD test depending on analyzed samples. The significance level was set at $p < 0.05$. Graphs were generated using GraphPad Prism. Statistical significance in the graphs is indicated by asterisks ($*p < 0.05$, $**p < 0.01$, $***p < 0.001$ and $****p < 0.0001$).

Approval for human experiments

Human-derived materials were preserved and handled with the approval and under the guidelines of French legislation. The accreditation number related to the use of human materials is DC- 2020–4203. Samples were stored in a biobank with authorization from the French Ministry of Health (Declaration number DC- 2008–304). Informed consent was obtained from all participants and/or their legal guardians.

Data availability

The datasets used and/or analysed during the current study are available from the corresponding author on reasonable request.

Received: 11 September 2024; Accepted: 1 April 2025
Published online: 13 August 2025

References

1. Jarvis, K., Assis-Nascimento, P., Mudd, L. M. & Montague, J. R. Beta-amyloid toxicity and reversal in embryonic rat septal neurons. *Neurosci. Lett* **423**, 184–188 (2007).
2. Schulte, S., Gries, M., Christmann, A. & Schäfer, K.-H. Using multielectrode arrays to investigate neurodegenerative effects of the amyloid-beta peptide. *Bioelectron. Med.* https://doi.org/10.1186/s42234-021-00078-4 (2021).
3. Pate, K. M. & Murphy, R. M. Cerebrospinal fluid proteins as regulators of beta-amyloid aggregation and toxicity. *Isr. J. Chem.* **57**, 602–612 (2017).
4. Menendez-Gonzalez, M. et al. Targeting beta-amyloid at the CSF: A new therapeutic strategy in alzheimer's disease. *Front. Aging Neurosci.* **10**, 1–8 (2018).
5. Sun, B. L. et al. Clinical research on alzheimer's disease: Progress and perspectives. *Neurosci. Bull.* **34**, 1111–1118. https://doi.org/10.1007/s12264-018-0249-z (2018).
6. McKhann, G. M. et al. The diagnosis of dementia due to Alzheimer's disease: Recommendations from the national institute on aging-Alzheimer's association workgroups on diagnostic guidelines for Alzheimer's disease. *Alzheimer's Dementia* **7**, 263–269 (2011).
7. Jack, C. R. et al. Revised criteria for diagnosis and staging of alzheimer's disease: Alzheimer's association workgroup. *Alzheimers Dement* https://doi.org/10.1002/alz.13859 (2024).
8. Alzheimer & Association. *Alzheimer's Association 2024 Alzheimer's Disease Facts and Figures*.
9. Jamerlan, A., An, S. S. A. & Hulme, J. Advances in amyloid beta oligomer detection applications in Alzheimer's disease. *TrAC - Trends Anal. Chem.* **129**, 115919 (2020).
10. Ameri, M. et al. Biosensors for detection of Tau protein as an Alzheimer's disease marker. *Int. J. Biol. Macromol.* **162**, 1100–1108 (2020).
11. Haes, A. J., Chang, L., Klein, W. L. & Van Duyne, R. P. Detection of a biomarker for Alzheimer's disease from synthetic and clinical samples using a nanoscale optical biosensor. *J. Am. Chem. Soc.* **127**, 2264–2271 (2005).
12. Theiss, S. et al. Dementia with Lewy bodies: Cerebrospinal fluid suppresses neuronal network activity. *NeuroReport* **28**, 1061–1065 (2017).
13. Amir, S., Arathi, A., Reshma, S. & Mohanan, P. V. Microfluidic devices for the detection of disease-specific proteins and other macromolecules, disease modelling and drug development: A review. *Int. J. Biol. Macromol.* https://doi.org/10.1016/j.ijbiomac.2023.123784 (2023).
14. Koch, H. et al. In vitro neuronal network activity as a new functional diagnostic system to detect effects of Cerebrospinal fluid from autoimmune encephalitis patients. *Sci. Rep.* **9**, 1–8 (2019).
15. Otto, F. et al. Cerebrospinal fluid of brain trauma patients inhibits in vitro neuronal network function via NMDA receptors. *Ann. Neurol.* **66**, 546–555 (2009).
16. Ren, Y. et al. A simple and reliable PDMS and SU-8 irreversible bonding method and its application on a microfluidic-MEA device for neuroscience research. *Micromachines (Basel)* **6**, 1923–1934 (2015).
17. Jokinen, V. et al. A microfluidic chip for axonal isolation and electrophysiological measurements. *J. Neurosci. Methods* **212**, 276–282 (2013).
18. Miny, L., Maisonneuve, B. G. C., Quadrio, I. & Honegger, T. Modeling neurodegenerative diseases using in vitro compartmentalized microfluidic devices. *Front. Bioeng. Biotechnol.* **10**, 1070 (2022).
19. McCready, F. P., Gordillo-Sampedro, S., Pradeepan, K., Martinez-Trujillo, J. & Ellis, J. Multielectrode arrays for functional phenotyping of neurons from induced pluripotent stem cell models of neurodevelopmental disorders. *Biology* https://doi.org/10.3390/biology11020316 (2022).
20. Toivanen, M. et al. Optimised PDMS tunnel devices on MEAs increase the probability of detecting electrical activity from human stem cell-derived neuronal networks. *Front. Neurosci.* https://doi.org/10.3389/fnins.2017.00606 (2017).
21. Kanagasabapathi, T. T., Ciliberti, D., Martinoia, S., Wadman, W. J. & Decré, M. M. J. Dual-compartment neurofluidic system for electrophysiological measurements in physically segregated and functionally connected neuronal cell culture. *Front. Neuroeng.* https://doi.org/10.3389/fneng.2011.00013 (2011).
22. Dworak, B. J. & Wheeler, B. C. Novel MEA platform with PDMS microtunnels enables the detection of action potential propagation from isolated axons in culture. *Lab Chip* **9**, 404–410 (2009).
23. Kutzing, M. K., Luo, V. & Firestein, B. L. Measurement of synchronous activity by microelectrode arrays uncovers differential effects of sublethal and lethal glutamate concentrations on cortical neurons. *Ann. Biomed. Eng.* **39**, 2252–2262 (2011).
24. Biffi, E. et al. Validation of long-term primary neuronal cultures and network activity through the integration of reversibly bonded microbioreactors and MEA substrates. *Biotechnol. Bioeng.* **109**, 166–175 (2012).
25. Bardy, C. et al. Neuronal medium that supports basic synaptic functions and activity of human neurons in vitro. *Proc. Natl. Acad. Sci. U S A* **112**, E2725–E2734 (2015).
26. Pigareva, Y. et al. Experimental platform to study spiking pattern propagation in modular networks in vitro. *Brain Sci.* https://doi.org/10.3390/brainsci11060717 (2021).
27. Gladkov, A. et al. Design of cultured neuron networks in vitro with predefined connectivity using asymmetric microfluidic channels. *Sci. Rep.* https://doi.org/10.1038/s41598-017-15506-2 (2017).
28. Goshi, N. et al. Influence of microchannel geometry on device performance and electrophysiological recording fidelity during long-term studies of connected neural populations. *Lab Chip* **22**, 3961–3975 (2022).
29. Heikkilä, T. J. et al. Human embryonic stem cell-derived neuronal cells form spontaneously active neuronal networks in vitro. *Exp. Neurol.* **218**, 109–116 (2009).
30. Hu, W. T. et al. CSF beta-amyloid 1–42 – what are we measuring in Alzheimer's disease?. *Ann. Clin. Transl. Neurol.* **2**, 131–139 (2015).
31. Ryan, D. A., Narrow, W. C., Federoff, H. J. & Bowers, W. J. An improved method for generating consistent soluble amyloid-beta oligomer preparations for in vitro neurotoxicity studies. *J. Neurosci. Methods* **190**, 171–179 (2010).
32. Uzoechi, S. C. et al. Effects of amyloid beta (Aβ) oligomers on blood-brain barrier using a 3D microfluidic vasculature-on-a-chip model. *Appl. Sci. (Switzerland)* https://doi.org/10.3390/app14093917 (2024).
33. Deleglise, B. et al. B-Amyloid induces a dying-back process and remote trans-synaptic alterations in a microfluidic-based reconstructed neuronal network. *Acta Neuropathol. Commun.* **2**, 1–9 (2014).
34. Li, W. et al. Investigation of the subcellular neurotoxicity of amyloid- β using a device integrating microfluidic perfusion and chemotactic guidance. *Adv. Healthc. Mater.* **201600895**, 1–8 (2017).

35. Ruiz, A. et al. Testing Aβ toxicity on primary CNS cultures using drug-screening microfluidic chips. *Lab Chip* **14**, 2860–2866 (2014).
36. Kilinc, D. et al. Pyk2 overexpression in postsynaptic neurons blocks Aβ 1-42-induced synaptotoxicity in a microfluidic co-culture model. *Brain Commun.* **2**(2), fcaa139. https://doi.org/10.1093/braincomms/fcaa139 (2020). PMID: 33718872; PMCID: PMC7941669.
37. Lefebvre, C. et al. Integration of microfluidic devices with microelectrode arrays to functionally assay amyloid-β-induced synaptotoxicity. *ACS Biomater. Sci. Eng.* **10**, 1856–1868 (2024).
38. Lopes, C. D. F., Mateus, J. C. & Aguiar, P. Interfacing microfluidics with microelectrode arrays for studying neuronal communication and axonal signal propagation. *J. Vis. Exp.* **2018**, 1–8 (2018).
39. Yaka, E. et al. Biological markers in cerebrospinal fluid (CSF) and evaluation of in vitro effect of CSF on PC12 cell line viability in Alzheimer's disease. *Cell Biochem. Funct.* **27**, 395–401 (2009).
40. Eriksdotter, M. et al. Cerebrospinal fluid from Alzheimer patients affects cell-mediated nerve growth factor production and cell survival in vitro. *Exp. Cell Res.* **371**, 175–184 (2018).
41. Jankeviciute, S. et al. Cerebrospinal fluids from Alzheimer's disease patients exhibit neurotoxic effects on neuronal cell cultures. *Eur. J. Neurosci.* **50**, 1994–2006 (2019).
42. Schiess, M. C. et al. CSF from parkinson disease patients differentially affects cultured microglia and astrocytes. *BMC Neurosci.* **11**, 151 (2010).
43. Chen, Y. A., Wang, K. C., Liu, D. Z., Young, T. H. & Tsai, L. K. The proliferation capacity of cultured neural stem cells promoted by CSF collected from SAH patients correlates to clinical outcome. *Sci. Rep.* **8**, 5–13 (2018).
44. Lehtinen, M. K. et al. The cerebrospinal fluid provides a proliferative niche for neural progenitor cells. *Neuron* **69**, 893–905 (2011).
45. Buddensiek, J. et al. Cerebrospinal fluid promotes survival and astroglial differentiation of adult human neural progenitor cells but inhibits proliferation and neuronal differentiation. *BMC Neurosci.* https://doi.org/10.1186/1471-2202-11-48 (2010).
46. Izsak, J., Seth, H., Theiss, S., Hanse, E. & Illes, S. Human cerebrospinal fluid promotes neuronal circuit maturation of human induced pluripotent stem cell-derived 3D neural aggregates. *Stem Cell Rep.* **14**, 1044–1059 (2020).
47. Kee Kwong, Ng. et al. Cerebrospinal fluid cytotoxicity in amyotrophic lateral sclerosis: a systematic review of in vitro studies. *Brain Commun.* **2**, 6–7 (2020).
48. Gomez-Pinedo, U. et al. Cellular changes in motor neuron cell culture produced by cytotoxic cerebrospinal fluid from patients with amyotrophic lateral sclerosis. *Neurología (English Edition)* **29**, 346–352 (2014).
49. Le, W. D., Rowe, D. B., Jankovic, J., Xie, W. & Appel, S. H. Effects of cerebrospinal fluid from patients with parkinson disease on dopaminergic cells. *Arch. Neurol.* **56**, 194–200 (1999).
50. Mandybur, G. T., Miyagi, Y., Yin, W., Perkins, E. & Zhang, J. H. Cytotoxicity of ventricular cerebrospinal fluid from parkinson patients: Correlation with clinical profiles and neurochemistry. *Neurol. Res.* **25**, 104–111 (2003).
51. Hao, R., Norgren, R. B., Lau, Y. S. & Pfeiffer, R. F. Cerebrospinal fluid of parkinson's disease patients inhibits the growth and function of dopaminergic neurons in culture. *Neurology* **45**, 138–142 (1995).
52. Görtz, P. et al. Multielectrode array analysis of cerebrospinal fluid in Alzheimer's disease versus mild cognitive impairment: A potential diagnostic and treatment biomarker. *Biochem. Biophys. Res. Commun.* **434**, 293–297 (2013).
53. Blennow, K. A review of fluid biomarkers for Alzheimer's disease: Moving from CSF to blood. *Neurol. Ther.* **6**, 15–24 (2017).
54. De Oliveira, T. R. et al. Early diagnosis of Alzheimer's disease in blood using a disposable electrochemical microfluidic platform. *ACS Sens* **5**, 1010–1019 (2020).
55. Kim, K. et al. Clinically accurate diagnosis of Alzheimer's disease via multiplexed sensing of core biomarkers in human plasma. *Nat. Commun.* https://doi.org/10.1038/s41467-019-13901-z (2020).
56. Li, Y. et al. Microfluidics-based systems in diagnosis of Alzheimer's disease and biomimetic modeling. *Micromachines* https://doi.org/10.3390/MI11090787 (2020).
57. Courte, J. *et al.* Reconstruction of directed neuronal networks in a microfluidic device with asymmetric microchannels. in *Methods in Cell Biology* 148 71–95 (Elsevier Inc., 2018).
58. Peyrin, J. M. et al. Axon diodes for the reconstruction of oriented neuronal networks in microfluidic chambers. *Lab Chip* **11**, 3663–3673 (2011).
59. Holloway, P. M. et al. Asymmetric confinement for defining outgrowth directionality. *Lab Chip* **19**, 1484–1489 (2019).
60. Renault, R., Durand, J. B., Viovy, J. L. & Villard, C. Asymmetric axonal edge guidance: A new paradigm for building oriented neuronal networks. *Lab Chip* **16**, 2188–2191 (2016).
61. Bradley, J. A. et al. Human induced pluripotent stem cell-derived glutamatergic neurons : Evaluating maturation and neurotoxic predictability in the presence or absence of GABAergic neurons and astrocytes using a microelectrode array platform. *Cyprotex Poster* **1**, 1 (2017).
62. Li, Y. et al. Implications of GABAergic neurotransmission in Alzheimer's disease. *Front. Aging Neurosci.* **8**, 1–12 (2016).
63. Benarroch, E. E. Glutamatergic synaptic plasticity and dysfunction in Alzheimer disease: Emerging mechanisms. *Neurology* **91**, 125–132 (2018).
64. Honegger, T., Thielen, M. I., Feizi, S., Sanjana, N. E. & Voldman, J. Microfluidic neurite guidance to study structure-function relationships in topologically-complex population-based neural networks. *Sci. Rep.* https://doi.org/10.1038/srep28384 (2016).
65. Fuchs, Q. et al. Co-culture of glutamatergic neurons and pediatric high-grade glioma cells into microfluidic devices to assess electrical interactions. *J. Vis. Exp.* https://doi.org/10.3791/62748 (2021).
66. Vanderstichele, H. et al. Standardization of preanalytical aspects of cerebrospinal fluid biomarker testing for Alzheimer's disease diagnosis: A consensus paper from the Alzheimer's biomarkers standardization initiative. *Alzheimer's Dementia* **8**, 65–73. https://doi.org/10.1016/j.jalz.2011.07.004 (2012).

Acknowledgements

The authors received no specific funding for this work.

Author contributions

Conceptualization, L.M., T.H. and I.Q.; experiments, L.M., L.D., A.B.; electrophysiological analyses, L.M.; data analyses: L.M.; A.P.; validation, L.M., J.R., F.L., I.Q. and T.H.; writing, L.M.; review, T.H., B.M., S.R., I.Q.

Declaration

Competing interests

T.H. is the Chief Executive Officer of NETRI, F.L. is the Chief Technological Officer of NETRI, L.M., J.R., A.B., L.D., B.M., S.R., H.G., R.T., and A.P. are employees of NETRI. N.V. is the Chief Executive Officer of ETAP-Lab, A.A., is an employee of ETAP-Lab. Other authors do not declare any conflict of interest.

Additional information

Supplementary Information The online version contains supplementary material available at https://doi.org/10.1038/s41598-025-97186-x.

Correspondence and requests for materials should be addressed to T.H. or I.Q.

Reprints and permissions information is available at www.nature.com/reprints.

Publisher's note Springer Nature remains neutral with regard to jurisdictional claims in published maps and institutional affiliations.